Journal of Molecular Structure 1245 (2021) 131067

Contents lists available at ScienceDirect

Journal of Molecular Structure

journal homepage: www.elsevier.com/locate/molstr

Synthesis, crystal structure, DFT, α-glucosidase and α-amylase inhibition and molecular docking studies of (E)-*N*'-(4-chlorobenzylidene)-5-phenyl-1H-pyrazole-3-carbohydrazide

Khalid Karrouchi[a,*], Saad Fettach[b], El Hassane Anouar[c], Burak Tüzün[d], Smaail Radi[e], Abdulrahman I. Alharthi[c], Hazem A. Ghabbour[f], Yahia N. Mabkhot[g], My El Abbes Faouzi[b], M'hammed Ansar[h], Yann Garcia[i,*]

[a] Laboratory of Analytical Chemistry and Bromatology, Faculty of Medicine and Pharmacy, Mohammed V University in Rabat, Morocco
[b] Laboratory of Pharmacology and Toxicology, Biopharmaceutical and toxicological analysis research team, Faculty of Medicine and Pharmacy Mohammed V University in Rabat, Morocco
[c] Department of Chemistry, College of Science and Humanities in Al-Kharj, Prince Sattam bin Abdulaziz University, Al-Kharj 11942, Saudi Arabia
[d] Science Faculty, Department of Chemistry, Cumhuriyet University, Sivas 58140, Turkey
[e] Laboratoire de Chimie Appliquée et Environnement (LCAE), Faculté des Sciences, Université Mohammed I, 60000 Oujda, Morocco
[f] Department of Medicinal Chemistry, Faculty of Pharmacy, University of Mansoura, Mansoura 35516, Egypt
[g] Department of Pharmaceutical Chemistry, College of Pharmacy, King Khalid University, Abha 61421, P. O. Box 960, 61421, Saudi Arabia
[h] Laboratory of Medicinal Chemistry, Faculty of Medicine and Pharmacy, Mohammed V University in Rabat, Morocco
[i] Institute of Condensed Matter and Nanosciences, Molecular Chemistry, Materials and Catalysis (IMCN/MOST), Université catholique de Louvain, Place L. Pasteur 1, 1348 Louvain-la-Neuve, Belgium

ARTICLE INFO

Article history:
Received 8 February 2021
Revised 30 June 2021
Accepted 6 July 2021
Available online 12 July 2021

Keywords:
Pyrazole
Crystal structure
DFT calculations
α-glucosidase
α-amylase
Molecular docking

ABSTRACT

In this work, a novel crystal i.e. (*E*)-*N*'-(4-chlorobenzylidene)-5-phenyl-*1H*-pyrazole-3-carbohydrazide has been synthesized and characterized using various spectroscopic techniques. The (*E*)-configuration of the azomethine (*N*=CH) was confirmed by single crystal X-ray analysis. The molecule crystallizes in the monoclinic space group, P21/c, a = 15.629(9) Å, b = 7.152(4) Å, c = 14.707(9) Å, β = 111.061(15)°, V = 1534.1(6) Å^3 and Z = 4. In addition, the elucidated molecular structure was confirmed by comparing the predicted Z-matrix geometries and spectroscopic data with the experimental ones. DFT calculations have been carried out in gas and IEFPCM solvent at the B3LYP/6–31+*G*(d,p). The *in vitro* anti-diabetic potential of the title compound was evaluated against α-glucosidase and α-amylase enzymes. Molecular docking studies showed that the various interactions tightly anchored the title compound to the active site, which makes it a more potent α-glucosidase inhibitor compared to well-known Acarbose.

1. Introduction

Diabetes mellitus (DM) is a group of metabolic diseases characterized by chronic hyperglycemia that leads to long-term macrovascular and microvascular complications [1]. Hence, one of the therapeutic approaches in treating diabetes is to reduce post-prandial hyperglycemia by inhibiting major carbohydrate hydrolyzing enzymes. α-glucosidase and α-amylase are the key carbohydrate hydrolyzing enzymes, located in the brush-border surface membrane of human intestinal cells, which plays an important role in the carbohydrate digestion [2]. Thus, discovery and development of new α-glucosidase and α-amylase inhibitors have attracted great attention in recent years.

Pyrazole is among a wide variety of heterocycles studied for the development of new active molecules. A systematic investigation of this class of compounds revealed that pyrazole can be traced in a number of well-established drugs belonging to different categories with diverse therapeutic activities [3-5] and pesticides [6, 7]. In the last few decades, the chemistry of pyrazole and their derivatives have received considerable attention owing to their wide spectrum of pharmacological activities including anti-diabetic agents, antibacterial, analgesics & anti-inflammatory, antioxidants, anti-cancer, antiviral, antidepressants, anti-alzheimer, anti-tubercular and anti-leishmanial [8-19]. Given the pharmacological properties of these derivatives, the study of their molecular structure, spectroscopic and electronic properties is fundamental to know the in-

* Correspondence authors: .
E-mail addresses: khalid.karrouchi@um5s.net.ma (K. Karrouchi), yann.garcia@uclouvain.be (Y. Garcia).

https://doi.org/10.1016/j.molstruc.2021.131067
0022-2860/

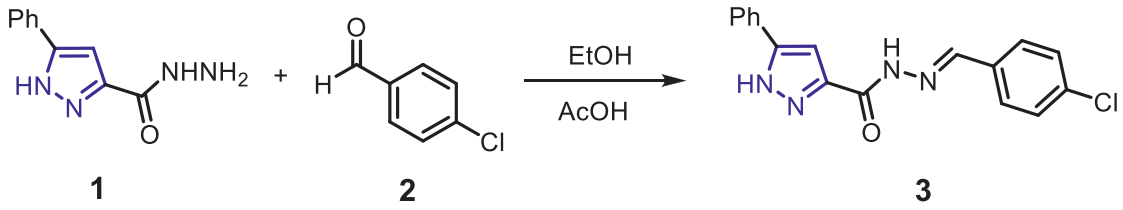

Scheme 1. Synthesis of compound **3**.

fluence of the different groups on the structures in order to discover the relationship of these groups with their biological properties. In this context, computational approaches have been known for their efficiency and accuracy when it comes to the prediction and understanding of properties of newly synthetized organic molecules [20-26]. In this work, we report the synthesis of (*E*)-*N*'-(4-chlorobenzylidene)−5-phenyl-*1H*-pyrazole-3-carbohydrazide (3) as new potent α-glucosidase and α-amylase inhibitor. The chemical structure of the title compound was characterized by FT-IR, ^{1}H NMR, ^{13}C NMR, ESI-MS and the (*E*)-configuration of its imine functionality (*N*=CH) was confirmed by single crystal X-ray analysis. In addition, the electronic characters and molecular geometry of this molecule were explored thanks to DFT calculations. Molecular docking simulations and Hirshfeld surface analysis were also performed for the title molecule. Its *in vitro* antidiabetic activity was evaluated against α-glucosidase and α-amylase enzymes, and compared to acarbose.

2. Materials and methods

2.1. General

All chemicals were purchased from Sigma-Aldrich. Reactions were checked with TLC using aluminum sheets with silica gel 60 F254 from Merck. Melting points were measured using a Büchi B-545 digital capillary melting point apparatus (BUCHI Labortechnik AG, Flawil, CH, Switzerland) and used without correction. The FT-IR spectrum was recorded with a Perkin-Elmer VERTEX 70 FT-IR spectrometer covering field 400–4000 cm^{-1}. ^{1}H and ^{13}C NMR spectra were recorded in solution in DMSO–d_6, on a Bruker spectrometer (300 MHz). Chemical shifts are expressed in parts per million (ppm) by using tetramethylsilane (TMS) as internal reference. Mass spectra were collected using API 3200 LC/MS/MS system, equipped with an ESI source.

2.2. Synthesis

The title compound was synthesized following the reported procedure [27-29].To a solution of 5-phenyl-1H-pyrazole-3-carbohydrazide (1) (1 mmol) in EtOH (10 mL) was added an equimolar amount of 4-chlorobenzaldehyde (2) in the presence of two drops of acetic acid. The mixture was maintained under reflux for 2 h. Then, the reaction mixture was poured in cold water, and the precipitate formed was filtered out, washed with ethanol and recrystallized from ethanol providing white crystals. 363 mg, Yield 89%; m.*p* = 301–303 °C; FT-IR (ATR, ν(cm^{-1})): 3391, 3320 (NH), 1666 (*C* = *O*), 1604, 1588 (*C* = *N*); 1461–1563 (*C* = *C*); ^{1}H NMR (300 MHz, DMSO–d_6, δ(ppm)): δ = 7.11 (s, 1H, H-pyrazole), 7.33–7.60 (m, 5H, H-pH), 7.59 (d, *J* = 7.8 Hz, 2H, H-Ar), 7.81 (d, *J* = 7.8 Hz, 2H, H-Ar), 8.46 (s, 1H, -*N*=CH), 11.65 (s, 1H, NHCO) 13.79 (s, 1H, NH-pyrazole); ^{13}C NMR: (75 MHz, DMSO–*d6*, δ (ppm)): 103.82, 125.82, 127.53, 127.90, 128.99, 129.49; 129.91, 132.18, 136.8, 140.28, 146.18, 148.20, 156.88, 158.62, 164.13. ESI-MS: *m/z* = 325.2 [*M* + *H*]$^+$, 347.3 [*M*+Na]$^+$.

2.3. X-ray crystallographic analysis

Single crystals of 3 were obtained by slow evaporation from an ethanol solution of the product at room temperature. Cell refinement and data reduction were carried out by Bruker SAINT. SHELXT was used to solve the crystal structure [30, 31]. The final refinement was carried out by full-matrix least-squares techniques with anisotropic thermal data for no hydrogen atoms on F. CCDC 1836580 for 3, contain the supplementary crystallographic data, which can be obtained free of charge from the Cambridge Crystallographic Data centre via http://www.ccdc.cam.ac.uk/data_request/cif. Scheme 1.

2.4. Antidiabetic activity

The α-glucosidase and α-amylase inhibition assays were conducted according to previously reported protocols [32].

2.5. DFT details

Geometry optimization and frequency calculations of the ground state (GS) of 3 has been carried out at the B3LYP/6–31+*G*(d,p) of theory as implemented in the Gaussian 16 software package [33]. The experimental X-ray coordinates 3 were used as the starting input coordinates for DFT calculations without constraints. The ground state minimum for 3 was confirmed by the absence of imaginary frequencies. The calculated vibrational modes were scaled by 0.9679 [34]. The predicted ^{1}H and ^{13}C NMR chemical shifts were obtained within the GIAO approach [35, 36] by calculating the isotropic chemical shielding constants at the same level of theory. The isotropic shielding constants were used to calculate the isotropic chemical shifts, δ_{cal}, with respect to tetramethylsilane (TMS). δ_{iso}= ρ_{TMS} − ρ_{iso}, where δ_{iso}, $\rho_{iso}$and ρ_{TMS} are the chemical shift, the absolute shielding and the absolute shielding of TMS, respectively. Solvent effects were taken into account implicitly using the integral equation formalism (IEF-PCM) [37]. In this model, the substrate is embedded into a cavity surrounded by a dielectric continuum characterized by its dielectric constant (ε(DMSO) = 46.826) [37].

2.6. Hirshfeld surface calculations

The analyses of the Hirshfeld surface and fingerprint plots of 3 were obtained using the Crystal Explorer 3.0 package [38]. The d_{norm} plots were mapped with color scale range − 0.51 au (blue) and 1.34 au (red). The red spots on the Hirshfeld surface indicate the interactions involving hydrogen bonds. Two-dimensional (2D) fingerprints were plotted using the expanded 0.6–2.8 Å range, with d_e and d_i scales displayed on the plot axes, where d_e and d_i represent the distances to the nearest nuclei outside and inside the surface from the Hirshfeld surface, respectively.

2.7. Molecular docking

Molecular docking of 3 into the active sites of α-glucosidase and α-amylase has been achieved using Autodock package [39]. X-

Table 1
Refinement parameters and crystal data for **3**.

Crystal data	
Molecular Formula	$C_{17}H_{13}ClN_4O$
Molecular Weight	324.76
Crystal System, Space Group	Monoclinic, $P2_1/c$
T (K)	293
a, *b*, *c* (Å)	15.629(9), 7.152(4), 14.707(9)
β (°)	111.061(15)
V (Å^3)	1534.1(16)
Z	4
Radiation type	Mo Kα
μ (mm^{-1})	0.26
Crystal size (mm^3)	0.57 × 0.31 × 0.04

Data collection	
Diffractometer	Bruker APEX-II CCD
Absorption correction	Multi-scan, SADABS Bruker 2014
T_{min}, T_{max}	0.883, 0.921
No. of measured, independent and observed Reflections [$I > 2\sigma(I)$]	30,380, 2705, 1104
R_{int}	0.405

Refinement	
$R[F^2 > 2\sigma(F^2)]$, w$R(F^2)$, S	0.112, 0.275, 1.05
No. of reflections	2705
No. of parameters	217
H-atom treatment	H atoms treated by a mixture of independent and constrained refinement
$\Delta_{\rho max}$, $\Delta_{\rho min}$ (e Å^{-3})	0.63, −0.52

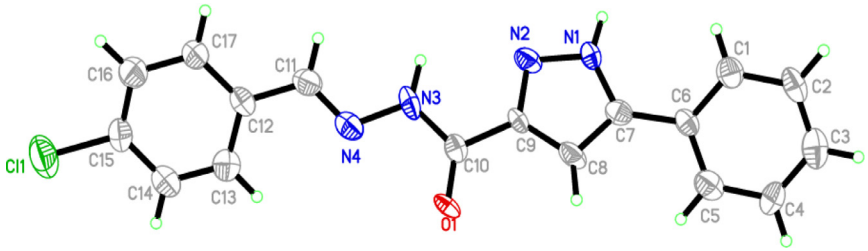

Fig. 1. Asymmetric unit of **3**.

ray coordinates of α-glucosidase and α-amylase and the original docked ligand acarbose were downloaded from the RCSB data bank web site with PDB codes 3W37 and 1B2Y for α-glucosidase and α-amylase, respectively [40, 41]. The docking stepwise was reported in our previous study [42, 43].

3. Results and discussion

3.1. X-ray crystal structure description

The compound **3** was analyzed by single crystals X-ray diffraction. Refinement parameters and crystal data are listed in Table 1. Supplementary data are deposited at CCDC under deposition number 1836580.

The compound **3** was analysed by single crystal X-ray diffraction. The summary of crystallographic information is listed in Table 1. The title molecule crystallizes in the monoclinic system, space group $P2_1/c$, a = 15.629(9) Å, b = 7.152(4) Å, c = 14.707(9) Å, β = 111.061(15)°, V = 1534.1(6) Å^3 and Z = 4.

The molecular structure of the title molecule is composed of three rings. These rings are pyrazole, phenyl and 4-chlorobenzyl which are connected through a carbohydrazide group. Pyrazole is connected to phenyl group in the 5- position. In the following discussion, the molecular structure and atomic numbering scheme adopted for the present study was taken from the asymmetric unit (Fig. 1). The C–C bond lengths in the phenyl rings lie between 1.36(1)–1.40(1) Å. The C–C bond lengths in the pyrazole ring is C7-C8=1.364(8) Å and C8-C9=1.38(1) Å. In the pyrazole ring, the C–N bond lengths are N1-C7=1.344(9) Å, N2-C9 = 1.317(8) Å. The N–N bond length is found at 1.358(8) Å for N1-N2 and 1.382(9) Å for N3-N4. The $C = O$ bond length (C10-O1) of carbohydrazide group is found to be 1.208(8) Å. For the pyrazole moiety of the title compound, the bond angles N2-N1-C7, N1-C7-C8, C7-C8-C9, C8-C9-N2 and N1-N2-C9 are 113.0(5)°, 105.9(6)°, 105.8(3)°, 112.8(6)° and 103.1(5)°, respectively. The bond angles lie between 117.9(6)° and 121.7(7)° for phenyl rings. The torsion angles around the pyrazole group in the present case are N1-N2-C9-C8 = −0.5(7)°, N2-C9-C8-C7 = 0.4(8)°, C7-N1-N2-C9 = 0.5(7)°, C9-C8-C7-N1 = −0.1(7)° and N2-N1-C7-C8 = −0.2(8)°.

Some of the experimental X-ray and calculated bond lengths and angles as well as dihedral torsion angles of **3** are listed in Table 2. The optimized geometry of **3** was obtained at B3LYP/6–31+G(d,p). Z-matrix coordinates of the optimized geometry and the starting X-Ray geometry of **3** are given as supplementary materials. A superposition of the optimized geometry of **3** and its X-ray diffraction crystal structure show an excellent agreement between experimental and calculated data (Fig. 2). This agreement is confirmed by the relatively good correlations obtained between the calculated and X-ray z-matrix coordinates of correlation coefficients of 99.74, 99.62 and 99.73% for bond lengths, angles and torsion angles, respectively.

3.2. FT-IR spectral analysis

The experimental FT-IR spectrum of the title compound was recorded in a solid state using reflectance (ATR) mode and

Table 2
Experimental and calculated selected Z-matrix coordinates of **3**.*.

r (Å)				a (°)				d (°)			
	Cal	Exp	Δr (Å)		Cal	Exp	Δa (°)		Cal	Exp	Δd (°)
r1–2	120.3	120.4	0.1	a1–2–3	120	120	0	d1–2–3–4	0	−1	1
r2–3	119.6	119.6	0.0	a2–3–4	120	120	0	d2–3–4–5	0	1	1
r3–4	120.3	119.9	0.4	a3–4–5	120	120	0	D3–4–5–6	0	−1	0
r4–5	120.5	121.4	0.9	a4–5–6	121	121	1	D4–5–6–7	−180	−178	2
r5–6	119.7	118.9	0.8	a5–6–7	120	119	1	D5–6–7–8	27	19	7
r6–7	131.4	129.3	2.1	a6–7–8	131	129	2	D6–7–8–9	−180	−180	0
r7–8	105.1	105.2	0.2	a7–8–9	105	105	0	D8–9–12–13	−1	−6	5
r8–9	111.5	112.8	1.3	a8–9–10	112	113	1	D10–9–12–14	−1	−7	6
r9–10	104.4	103.1	1.3	a9–10–11	104	103	1	D9–12–14–15	180	179	1
r10–11	113.6	113.0	0.6	a10–11–7	114	113	1	D13–12–14–15	0	0	0
r9–12	127.0	124.0	3.0	a8–9–12	127	124	3	D12–14–15–16	180	170	9
r12–13	122.1	122.1	0.0	a9–12–13	122	122	0	D14–15–16–17	180	177	3
r12–14	124.1	123.3	0.8	a13–12–14	124	123	1	D15–16–17–18	0	−9	9
r14–15	121.3	119.0	2.4	a12–14–15	121	119	2	D16–17–18–19	−180	−177	3
r15–16	116.5	116.5	0.0	a14–15–16	117	117	0	D17–18–19–20	0	−2	2
R16–17	121.9	118.8	3.1	a15–16–17	122	119	3	D18–19–20–21	0	−1	1
r17–18	122.4	122.3	0.1	a16–17–18	122	122	0	D19–20–21–22	0	3	3
r18–19	120.7	120.9	0.2	a17–18–19	121	121	0	D18–19–20–23	180	179	1
r21–22	118.9	119.1	0.3	a20–21–22	119	119	0	D20–21–22–17	0	−2	2
r20–23	119.2	119.0	0.2	a19–20–23	119	119	0	D22–21–20–23	−180	−177	3

* r = Length; a = Angle; d = Dihedral angle.

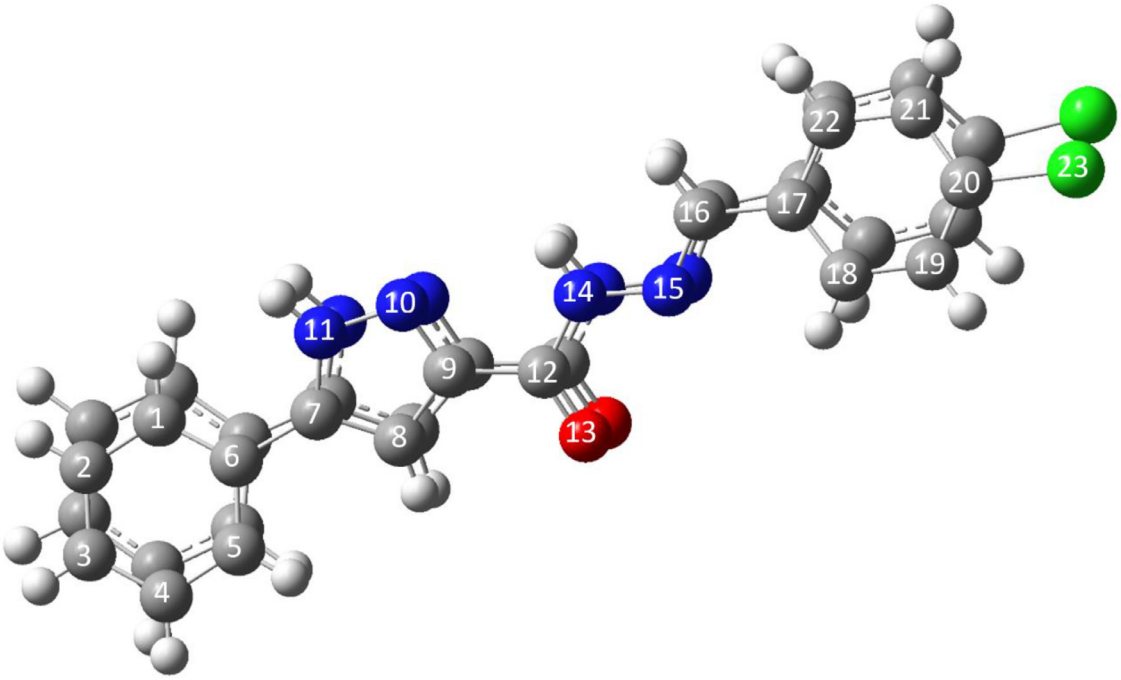

Fig. 2. Superposition of X-Ray crystal structure and optimized structure of **3**.

its comparison with the corresponding predicted in the gas phase by using the B3LYP/6–31+G(d,p) method are given in Fig. 3. The calculated vibration modes were calculated at the at the B3LYP/6–31+G(d,p) and scaled by a factor 0.9679 [34]. The N–H stretching vibrations are generally appears in the region 3500–3000 cm^{-1} [44-46]. The NH stretching band of pyrazole ring in (*E*)-*N*′–2,4-dichlorobenzylidene-5-phenyl-*1H*-pyrazole-3-carbohydrazide (E-DPPC) is reported at 3400 cm^{-1} [46]. For this molecule, the FT-IR band appears at 3391 cm^{-1} and 3320 cm^{-1} have been assigned to N–H stretching vibrations for pyrazole and carbohydrazide, respectively. The N–H in-plane deformation vibrations in pyrazole and carbohydrazide are reported at 1509 and 1386 cm^{-1}, respectively. Their corresponding predicted one were underestimated by 134 and 67 cm^{-1} (Table S1). In this case, the bands observed at 1438 and 1341 cm^{-1} are assigned as these modes in pyrazole and carbohydrazide. The C–H stretching vibrations of aromatic rings give rise to bands in the region 3200–3000 cm^{-1} in aromatic compounds [44-46]. Here, a series of bands between 3140 and 2831 cm^{-1} were assigned as CH stretching modes of the hydrazonoic group, 4-chlorobenzyl and phenyl rings. The $C = O$ stretching mode is usually one of the most representative in an infrared spectrum, it appears in a wavenumber region relatively free of other vibrations (1800–1600 cm^{-1}) [44-46]. This mode was reported at 1683 [46] and in this molecule, the $C = O$ stretching mode is assigned to the intense band at 1666 cm^{-1}. The CO stretching vibration is relatively well reproduced with a deviation of 14 cm^{-1} with respect to the observed value. The in-plane and the out-of-plane deformations of $C = O$ are reported at 905 and 757 cm^{-1}, respectively [46]. Here, the bands observed at 916 and 756 cm^{-1} are assigned to these modes. The $C = N$

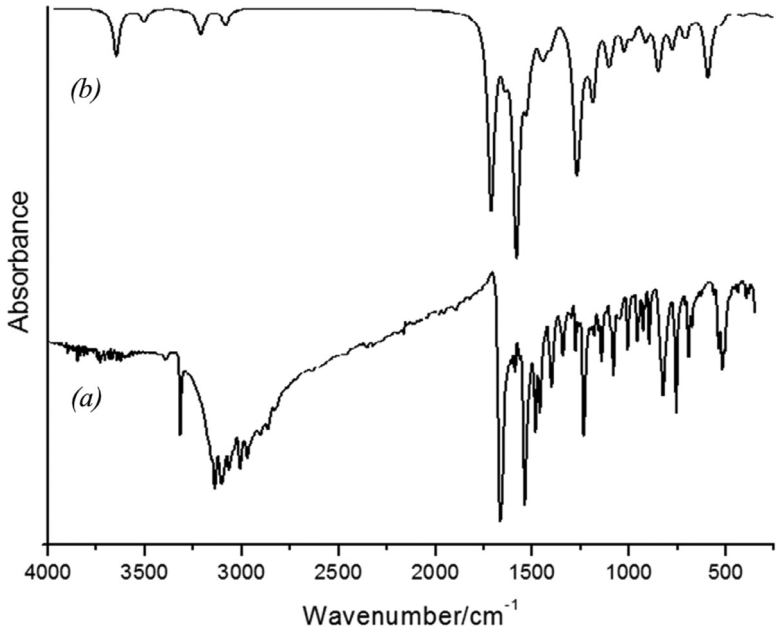

Fig. 3. Experimental (a) and calculated (b) FT-IR spectra of **3**.

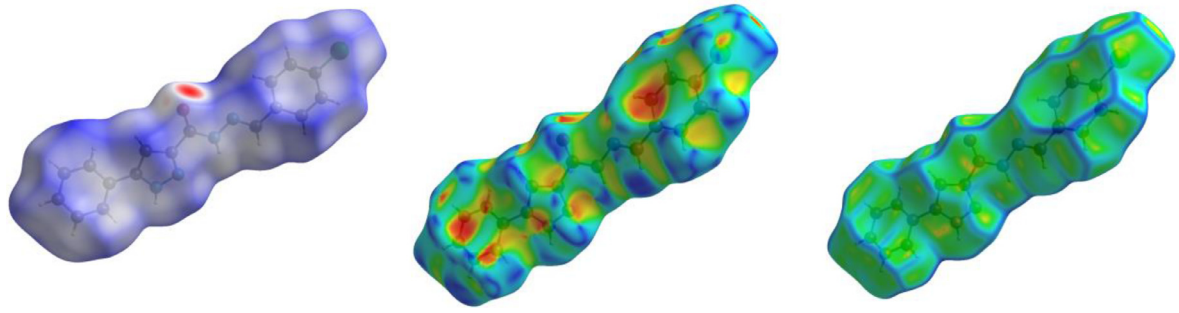

Fig. 4. Hirshfeld surface mapped over (a) d_{norm}, (b) shape-index and (c) curvedness of **3**.

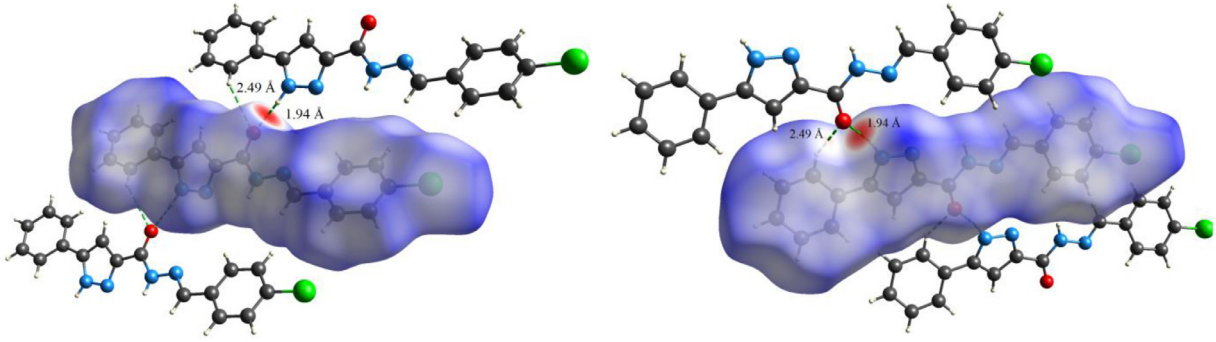

Fig. 5. d_{norm} mapped on the Hirshfeld surface for visualizing intermolecular hydrogen bonds established between **3** closest units.

stretching vibrations in pyrazole and carbohydrazide group are reported at 1593 and 1547 cm^{-1}, respectively [46]. For the title compound, the bands observed at 1604 and 1588 cm^{-1} are assigned as $C = N$ stretching mode in pyrazole and carbohydrazide group, respectively. The scaled stretching mode of $C = N$ carbohydrazide vibrates at 1588 cm^{-1} with a deviation of 34 cm-1 with respect to the experimental value. The aromatic $C = C$ stretching vibrations of pyrazole and phenyl ring are very much important and occur in the region 1200–1650 cm^{-1} [44-46]. For the studied molecule, a series of infrared bands having significant $C = C$ contributions were observed at 1461, 1484, 1539 and 1563 cm^{-1}.

3.3. ^{1}H & ^{13}C NMR studies

The experimental ^{1}H and ^{13}C NMR spectra of compound **3** were obtained by using TMS as an internal standard and DMSO–d_6 as solvent (Figs. S1 and S2, and Table S2). The predicted ^{1}H and ^{13}C NMR chemical shifts of **3** were obtained within the GIAO approach [35, 36] at the same level of theory, *i.e.,* at the B3LYP/6–31+*G*(d,p) and IEF-PCM. The experimental ^{1}H and ^{13}C NMR chemical shifts are relatively well reproduced. Indeed, the correlation curves between the experimental and predicted chemical shift yield correlation coefficients of 97.37 and 96.85% for ^{1}H and ^{13}C

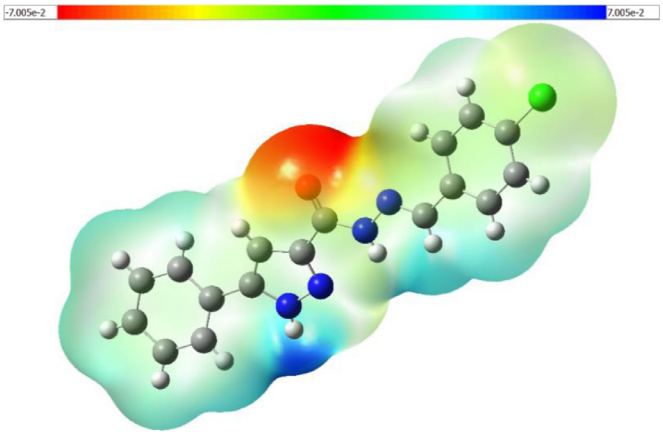

Fig. 6. EPS of **3** obtained at the B3LYP/6–311+*G*(d,p) level of theory.

NMR chemical shifts, respectively (Fig. S3). For the ^{1}H chemical shifts maximal and minimal deviations were obtained for CH-pyarazol ring and –*N*=CH protons of 0.12 and 0.05 ppm, respectively. While, for the ^{13}C chemical shifts maximal and minimal deviations were obtained for carbon nucleus of–*N*=CH and pyarazol ring of 25.49 and 19.77 ppm, respectively. The ^{1}H NMR spectrum of the title molecule displayed a singlet at δ = 7.11 ppm due to pyrazole proton (C4-H) and a multiplet at δ = 7.26–7.48 ppm due to phenyl protons. The predicted chemical shift of the pyrazole proton resonates at 7.23 ppm with a deviation of 0.12 ppm with respect to the observed value. The chemical shifts of the 4-chlorophenyl protons appeared as two doublets at δ = 7.59 ppm and δ = 7.81 ppm. The chemical shifts of the azomethine (-*N*=CH-) and amide (NHCO) protons appear as a singlet at δ = 8.46 and δ = 11.65 ppm, respectively. The chemical shifts of NH pyrazole proton appeared as singlet at δ = 13.79 ppm. The chemical shifts of the amide (NHCO) and NH pyrazole protons are relatively well reproduced with the variation of 1.20 and 0.68 ppm, respectively. The ^{13}C NMR spectra of the title compound showed the chemical shifts of *C* = *O* are at δ = 164.13 ppm. Its corresponding predicted chemical shifts resonates at 189.06 ppm with a deviation of 24.93 with respect to the experimental value. The signal at δ = 148.20 ppm are clearly assigned for azomethine group chemical shifts *C* = *N*. The signals at δ = 103.82, 156.88 and 158.62 ppm are assigned to pyrazole carbons, while that of the aromatic carbon chemical shifts occurred in the range of δ = 125.82–132.18 ppm.

3.4. ESI-MS study

The ESI-MS spectrum show molecular ion peaks with *m/z* = 325.2 corresponding to the molecular weight [*M* + *H*]+. The *m/z* = 347.2 correspond to the sodiated molecular ion peak [*M*+Na]+. These values are in good agreement with the proposed composition for the title molecule (C17H13ClN4O) (Fig. S4).

3.5. Hirshfeld surface studies

Hirshfeld surfaces mapped over dnorm, shape index and curvedness of 3 were obtained using Crystal Explorer 3.0 (Fig. 4). Internal and external (di and de) contact distances from the Hirshfeld surface to the nearest atom inside and outside enables the analysis of intermolecular interactions through the mapping of dnorm.

The red spots on Hirshfeld surface of **3** indicate the existence of intermolecular interactions (intercontacts) in the crystalline envi-

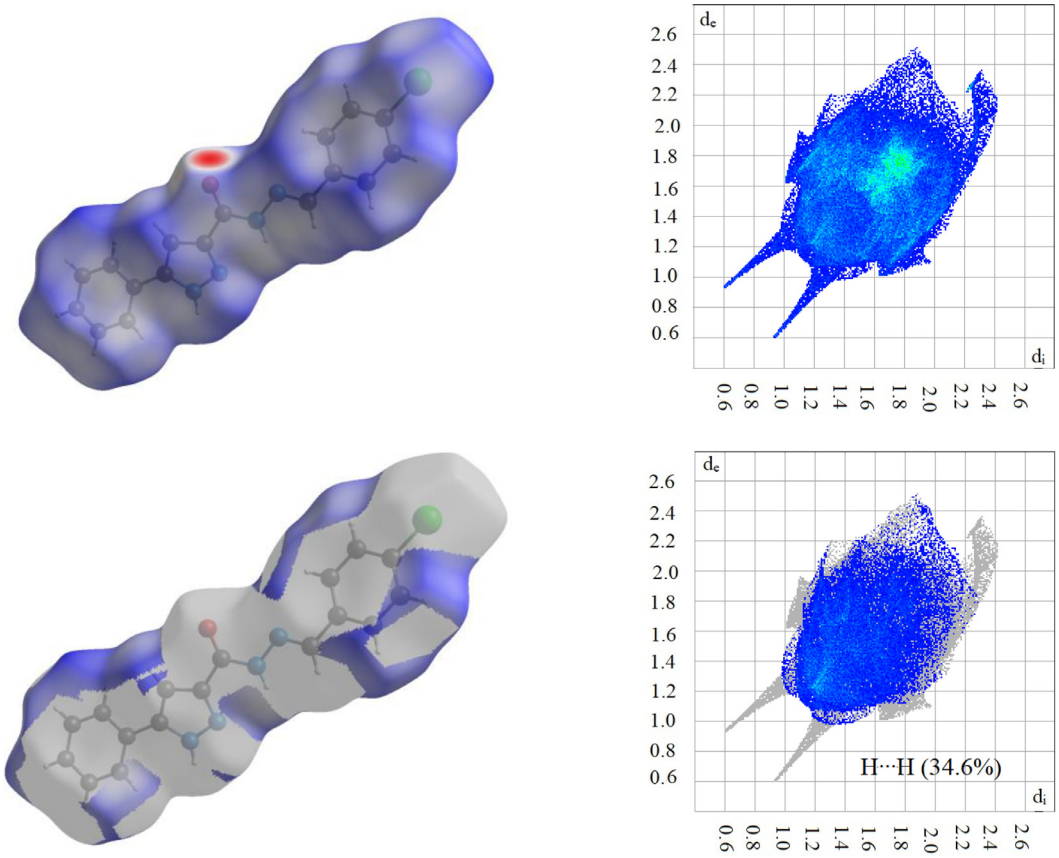

Fig. 7. 2D fingerprint plots for **3** showing closest intercontacts.

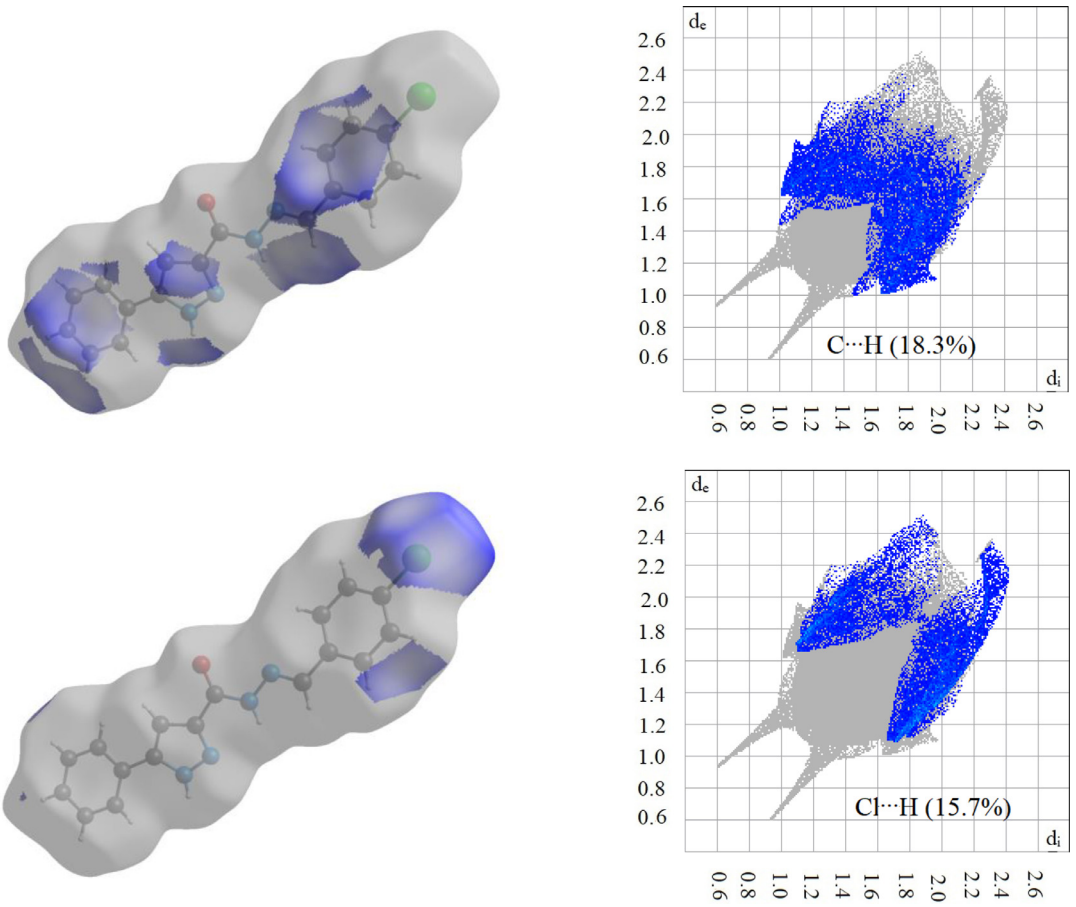

Fig. 7. Continued

ronment that involve hydrogen bonding (Fig. 5). Three intermolecular hydrogen bonds are identified between molecular units. The first one is established between the lone pair of carbonyl function in **3** and the hydrogen atom of the amine of pyrazole ring of another unit (1.94 Å). The second hydrogen bond is established between the lone pair of carbonyl function of **3** and the hydrogen atom of the CH aromatic ring at ortho position with respect to pyrazole ring of another unit (2.49 Å). The latest one is established between the hydrogen atom of the amine of pyrazole ring of **3** and lone pair of carbonyl function of another unit (1.94 Å).

The electrostatic surface potential of **3** is calculated using DFT at the B3LYP/6–31+*G*(d,p) level of theory (Fig. 6). The negative region on the electrostatic potential appears in red and corresponds to hydrogen bond acceptors, while the positive region on electrostatic potential appears in blue and corresponds to hydrogen-bond donors. As can be seen from Fig. 6, the carbonyl group corresponds to a hydrogen atom acceptor, whilst the amine group of pyrazole ring corresponds to hydrogen-bond donors (Fig. 5).

The 2D fingerprint plots for closest intercontacts of **3** are shown in Fig. 7 and summarized in Table 3. The highest interatomic contact contribution were found between hydrogen atoms H•••H (34.6%) (Fig. 7), followed by C•••H/H•••C and Cl•••H/H•••Cl with 18.3% and 15.7%, respectively.

Table 3
Summary of intercontacts and their percentage contributions to the Hirshfeld surface of **3**.

Type of contact	Contribution (%)
H···H	34.6
C···H/ H···C	18.3
Cl···H/ H···Cl	15.7
O···H/ H···O	8.9
N···H/ H···N	6.7
C···C	7.6
N···C/ C···N	4.7

Table 4
α-glucosidase and α-amylase inhibitory activities of **3.**

Compound	IC_{50} (μM)[a]	
	α-glucosidase	α-amylase
3	60.45 ± 1.23	32.13 ± 1.05
Acarbose	89.12 ± 2.08	2.29 ± 0.21

[a] Values are mean±SEM of three independent experiments.

3.6. Antidiabetic activity and molecular docking

The antidiabetic activity of **3** has been systematically evaluated against α-amylase and α-glucosidase by calculating its corresponding IC_{50} values. The IC_{50} values of the pyrazole derivative **3** were compared with two standard antidiabetic drugs, acarbose and pioglitazone. On one hand, **3** with IC_{50} = 60.45 ± 1.23 μM shows higher α-glucosidase inhibition efficiency compared with acarbose and pioglitazone (Table 4). On another hand, **3** with IC_{50} = 32.13 ± 1.05 μM shows lower activity towards α-amylase compared with acarbose, and higher activity compared with pioglitazone (Table 4). A molecular docking study was undertaken to determine and rationalize the binding modes between **3** and

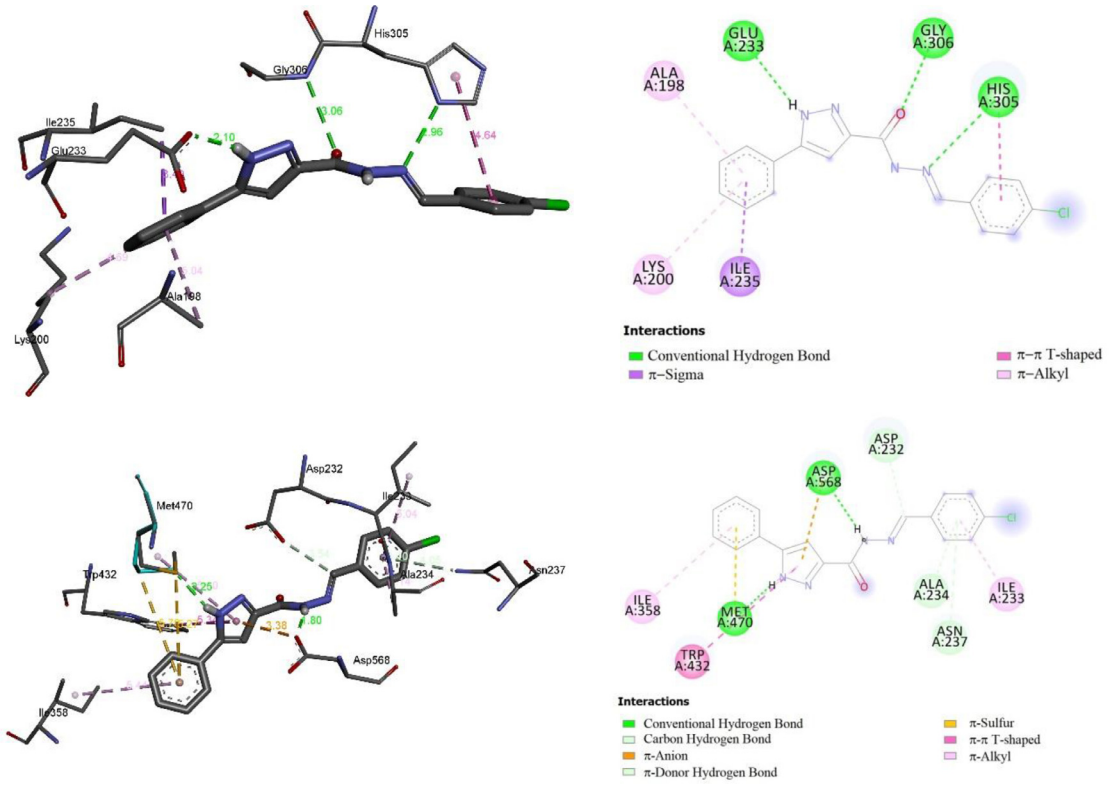

Fig. 8. Binding between the docked pyrazole derivative **3** and α-amylase and α-glucosidase.

α-glucosidase or α-amylase, respectively. Binding energies of the stable complexes **3**-α-glucosidase (or α-amylase), number of established intermolecular hydrogen bonding between **3** and active site residues of α-glucosidase (or α-amylase) were determined too. The complexes formed between **3** and amino acids into the binding site of α-glucosidase and α-amylase show negative bending energies of −7.88 and −6.72 kcal/mol, respectively. These values indicate that the inhibition of α-glucosidase and α-amylase by **3** is thermodynamically favorable. The stability of **3-**α-amylase complex mainly refer to hydrogen bonds, π-Sigma, π-π and π-alkyl intermolecular interactions established between **3** and the active amino acids of α-amylase (Fig. 8, up). Three hydrogen bonds are formed in **3-**α-amylase complex between lone pair of keto group of Glu 233 amino acid and hydrogen atom of pyrazole of **3**, hydrogen atom amine group of Gly 306 amino acid and the lone pair of oxygen atom of keto group of **3**, and hydrogen atom of the amine group in of His 305 amino acid and lone pair of nitrogen atom of imine functional of **3** at distances 2.10, 3.06 and 2.96 Å. π-π stacking intermolecular interaction are formed between π bonds of five member ring of His 305 amino acid and π bonds of chlorobenzene moiety of **3** at a distance 4.96 Å.

In **3-**α-glucosidase complex, many intermolecular interactions are established between the docked pyrazole and the active amino acids of α-glucosidase including conventional hydrogen bonds, carbon hydrogen bonds, π-Anion, π-Donor hydrogen bonds, π-Sulfur, π-π T-shaped and π-Alkyl interactions (Fig. 8, bottom). The two hydrogen bonds are formed in **3-**α-glucosidase complex between lone pair of sulfur atom of Met 470 amino acid and hydrogen atom of pyrazole of **3**, lone pair of oxygen atom of Asp 568 amino acid and hydrogen atom of the amine group of **3** at distances 2.56 and 180. Å. π-π T-shaped intermolecular interaction is formed between π bonds of five member ring of Trp 432 amino acid and π bonds of pyrazole moiety of **3** at a distance 5.34 Å. The carbon hydrogen bond is formed between the lone of oxygen atom of Asp 232 and the hydrogen atom attached to carbon atom of imine group at a distance 3.54 Å.

4. Conclusions

(*E*)-*N*'-(4-chlorobenzylidene)−5-phenyl-*1H*-pyrazole-3-carbohydrazide (**3**) has been synthesized and fully characterized using various spectroscopic techniques. Single crystal X-ray diffraction confirmed the (*E*)-configuration of the azomethine (*N*=CH) group of the title compound. The molecular geometry and electronic structure were optimized by DFT calculations. Hirshfeld surface analysis revealed the occurrence of intermolecular interactions in the crystalline state of the pyrazole **3** like H•••H, C•••H and Cl•••H bonding. The *in vitro* anti-diabetic potential of the title compound was evaluated against α-glucosidase and α-amylase enzymes. **3** with IC_{50} = 60.45 ± 1.23 μM shows higher α-glucosidase inhibition efficiency compared with acarbose (efficient against Type 2 diabets). Molecular docking studies revealed that various interactions tightly anchored the title compounds to the active site, which could well explain their excellent antidiabetic activities, compared to the reference drug Acarbose (IC_{50} = 89.12 ± 2.08 μM).

Author statement

Khalid Karrouchi: Conceptualization, Methodology, Writing - original draft, Writing - review & editing. **Saad Fettach and My El Abbes Faouzi:** α-glucosidase and α-amylase inhibiton studies. **El Hassane Anouar, Abdulrahman I. Alharthi and Burak Tüzün:** Theoretical Calculations, Writing - Original Draft. **Smaail Radi and M'hammed Ansar:** Supervision. **Hazem A. Ghabbour and Yahia N. Mabkhot:** X-ray data, Validation, Collected the data. **Yann Garcia**: Investigation.

Declaration of Competing Interest

The authors declare that they have no known competing financial interests or personal relationships that could have appeared to influence the work reported in this paper.

Acknowledgments

This work was also supported by PPR2-MESRSFC–CNRST-P10 project (Morocco) as well as the UM5R.The authors extend their appreciation to the Deanship of Scientific Research at King Khalid University for funding this work through Research Group Project under grant number (R.G.P. 2/26/42). We also thank the bilateral WBI-Morocco grant (COP 22 Program 2018– 2022) and the Fonds De La Recherche Scientifique—FNRS (CDR 33694457, PDR T.0095.21).

Supplementary materials

Supplementary material associated with this article can be found, in the online version, at doi:10.1016/j.molstruc.2021.131067.

References

[1] A.D. Deshpande, M. Harris-Hayes, M. Schootman, Epidemiology of diabetes and diabetes-related complications, Phys. Ther. 88 (2008) 1254–1264.
[2] H. Teng, L. Chen, α-Glucosidase and α-amylase inhibitors from seed oil: a review of liposoluble substance to treat diabetes, Crit. Rev. Food Sci. Nutr. 57 (2017) 3438–3448.
[3] M.F. Khan, M.M. Alam, G. Verma, W. Akhtar, M. Akhter, M. Shaquiquzzaman, The therapeutic voyage of pyrazole and its analogs: a review, Eur. J. Med. Chem. 120 (2016) 170–201.
[4] K. Karrouchi, S. Radi, Y. Ramli, J. Taoufik, Y. Mabkhot, F. Al-aizari, M. Ansar, Synthesis and Pharmacological Activities of Pyrazole Derivatives: a Review, Molecules 23 (2018) 134.
[5] F.E. Bennani, L. Doudach, Y. Cherrah, Y. Ramli, K. Karrouchi, M. Ansar, M.E.A. Faouzi, Overview of recent developments of pyrazole derivatives as an anticancer agent in different cell line, Bioorg. Chem. (2019) 103470.
[6] T.P. Selby, G.P. Lahm, T.M. Stevenson, K.A. Hughes, D. Cordova, I.B. Annan, T.F. Pahutski, Discovery of cyantraniliprole, a potent and selective anthranilic diamide ryanodine receptor activator with cross-spectrum insecticidal activity, Bioorg. Med. Chem. Lett. 23 (2013) 6341–6345.
[7] G.A. Herron, J. Rophail, Tebufenpyrad (Pyranica®) resistance detected in two-spotted spider mite Tetranychus urticae Koch (Acari: tetranychidae) from apples in Western Australia, Exp. Appl. Acarol. 22 (1998) 633–641.
[8] G. Bansal, S. Singh, V. Monga, P.V. Thanikachalam, P. Chawla, Synthesis and biological evaluation of thiazolidine-2, 4-dione-pyrazole conjugates as antidiabetic, anti-inflammatory and antioxidant agents, Bioorg. Chem. 92 (2019) 103271.
[9] K. Karrouchi, L. Chemlal, J. Taoufik, Y. Cherrah, S. Radi, M.-.E. Faouzi, M. Ansar, Synthesis, antioxidant and analgesic activities of Schiff bases of 4-amino-1, 2, 4-triazole derivatives containing a pyrazole moiety, Ann. Pharm. Fr. 74 (2016) 431–438.
[10] K. Karrouchi, S. Fettach, S. Radi, J. Taoufik, Y.N. Mabkhot, S. Alterary, My E.A. Faouzi, M. Ansar, Synthesis, Characterization, Free-radical Scavenging Capacity and Antioxidant Activity of Novel Series of Hydrazone, 1, 3, 4-oxadiazole and 1, 2, 4-triazole Derived from 3, 5-dimethyl-1H-pyrazole, Lett. Drug. Des. Discov. 16 (2019) 712–720.
[11] K. Chkirate, S. Fettach, K. Karrouchi, N.K. Sebbar, E.M. Essassi, J.T. Mague, S. Radi, M.E.A. Faouzi, N.N. Adarsh, Y. Garcia, Novel Co(II) and Cu(II) coordination complexes constructed from pyrazole-acetamide: effect of hydrogen bonding on the self assembly process and antioxidant activity, J. Inorg. Biochem. 191 (2019) 21–28.
[12] K. Chkirate, K. Karrouchi, N. Dege, N.K. Sebbar, A. Ejjoummany, S. Radi, N.N. Adarsh, A. Talbaoui, M. Ferbinteanu, E.M. Essassi, Y. Garcia, Co(ii) and Zn(ii) pyrazolyl-benzimidazole complexes with remarkable antibacterial activity, New J. Chem. 44 (2020) 2210–2221.
[13] F. Ran, Y. Liu, D. Zhang, M. Liu, G. Zhao, Discovery of novel pyrazole derivatives as potential anticancer agents in MCL, Bioorg. Med. Chem. Lett. 29 (2019) 1060–1064.
[14] Y. Wu, C. Tang, R. Rui, L. Yang, W. Ding, J. Wang, W. Xiao, Synthesis and biological evaluation of a series of 2-(((5-akly/aryl-1H-pyrazol-3-yl) methyl) thio)-5-alkyl-6-(cyclohexylmethyl)-pyrimidin-4 (3H)-ones as potential HIV-1 inhibitors, Acta Pharm. Sin. 10 (2020) 512–528.
[15] B. Mathew, J. Suresh, S. Anbazhagan, Synthesis, in silico preclinical evaluation, antidepressant potential of 5-substituted phenyl-3-(thiophen-2-yl)-4, 5-dihydro-1h-pyrazole-1-carboxamides, Biomed. Aging Pathol. 4 (2014) 327–333.
[16] K. Chkirate, S. Fettach, M. El Hafi, K. Karrouchi, B. Elotmani, J.T. Mague, S. Radi, M.E.A. Faouzi, N.N. Adarsh, E.M. Essassi, Y. Garcia, Solvent induced supramolecular polymorphism in Cu (II) coordination complex built from 1, 2, 4-triazolo [1, 5-a] pyrimidine: crystal structures and anti-oxidant activity, J. Inorg. Biochem. 208 (2020) 111092.
[17] Y. Xu, Z. Zhang, X. Jiang, X. Chen, Z. Wang, H. Alsulami, W. Tang, Discovery of δ-sultone-fused pyrazoles for treating Alzheimer's disease: design, synthesis, biological evaluation and SAR studies, Eur. J. Med. Chem. 181 (2019) 111598.
[18] Z. Xu, C. Gao, Q.-.C. Ren, X.-.F. Song, L.-.S. Feng, Z.-.S. Lv, Recent advances of pyrazole-containing derivatives as anti-tubercular agents, Eur. J Med. Chem. 139 (2017) 429–440.
[19] K. Figarella, S. Marsiccobetre, I. Galindo-Castro, N. Urdaneta, J. Herrera, N. Canudas, E. Galarraga, Antileishmanial and antitrypanosomal activity of synthesized hydrazones, pyrazoles, pyrazolo [1, 5-a]-pyrimidines and pyrazolo [3, 4-b]-pyridine, Curr. Bioact. Compd. 14 (2018) 234–239.
[20] R.R. Pillai, K. Karrouchi, S. Fettach, S. Armaković, S.J. Armaković, Y. Brik, J. Taoufik, S. Radi, M.E.A. Faouzi, M. Ansar, Synthesis, spectroscopic characterization, reactive properties by DFT calculations, molecular dynamics simulations and biological evaluation of Schiff bases tethered 1, 2, 4-triazole and pyrazole rings, J. Mol. Struct. 1177 (2019) 47–54.
[21] S. Tighadouini, R. Benabbes, M. Tillard, D. Eddike, K. Haboubi, K. Karrouchi, S. Radi, Synthesis, crystal structure, DFT studies and biological activity of (Z)-3-(3-bromophenyl)-1-(1,5-dimethyl-1H-pyrazol-3-yl)-3-hydroxyprop-2-en-1-one), Chem. Cent. J. 12 (2018) 122.
[22] Y. Bouzian, K. Karrouchi, Y. Sert, C.H. Lai, L. Mahi, N.H. Ahabchane, A. Talbaoui, J.T. Mague, E.M. Essassi, Synthesis, spectroscopic characterization, crystal structure, DFT, molecular docking and *in vitro* antibacterial potential of novel quinoline derivatives, J. Mol. Struct. 1209 (2020) 127940.
[23] F. El Kalai, E.B. Çınar, C.H. Lai, S. Daoui, T. Chelfi, M. Allali, N. Dege, K. Karrouchi, N. Benchat, Synthesis, spectroscopy, crystal structure, TGA/DTA study, DFT and molecular docking investigations of (E)-4-(4-methylbenzyl)-6-styrylpyridazin-3 (2H)-one, J. Mol. Struct. (2020) 129435.
[24] S. Daoui, C. Baydere, F. Akman, F. El Kalai, L. Mahi, N. Dege, Y. Topcu, K. Karrouchi, N. Benchat, Synthesis, X-ray crystallography, vibrational spectroscopy, thermal and DFT studies of (E)-6-(4-methylstyryl)-4, 5-dihydropyridazin-3 (2H)-one, J. Mol. Struct. 1225 (2020) 129180.
[25] F. El Kalai, K. Karrouchi, C. Baydere, S. Daoui, M. Allali, N. Dege, N. Benchat, S.A. Brandán, Synthesis, crystal structure, spectroscopic studies, NBO, AIM and SQMFF calculations of new pyridazinone derivative, J. Mol. Struct. 1223 (2020) 129213.
[26] K. Karrouchi, E.B. Yousfi, N.K. Sebbar, Y. Ramli, J. Taoufik, Y. Ouzidan, M. Ansar, Y.N. Mabkhot, H.A. Ghabbour, S. Radi, New Pyrazole-Hydrazone Derivatives: x-ray Analysis, Molecular Structure Investigation via Density Functional Theory (DFT) and Their High In-Situ Catecholase Activity, Int. J. Mol. Sci. 18 (2017) 2215.
[27] K. Karrouchi, S. Radi, J. Taoufik, H.A. Ghabbour, Y.N. Mabkhot, Crystal structure of N′-(4-methoxybenzylidene)-5-phenyl-1H-pyrazole-3-carbohydrazide, C18H16N4O2, Z. Kristallogr. NCS. 231 (2016) 835–837.
[28] K. Karrouchi, S. Radi, J. Taoufik, H.A. Ghabbour, Y.N. Mabkhot, Crystal structure of N′-(4-nitrobenzylidene)-5-phenyl-1H-pyrazole-3-carbohydrazide, C17H13N5O3, Z. Kristallogr. NCS. 231 (2016) 839–841.
[29] K. Karrouchi, S. Radi, J. Taoufik, H.A. Ghabbour, Y.N. Mabkhot, Crystal structure of N′-(4-(dimethylamino) benzylidene)-5-phenyl-1H-pyrazole-3-carbohydrazide, C19H19N5O, Z. Kristallogr. NCS. 231 (2016) 883–886.
[30] G.M. Sheldrick, A short history of SHELX, Acta Crystallogr 64 (2008) 112–122.
[31] G.M. Sheldrick, Program SHELXTL97, Siemens Analytical X-ray Instruments, Inc., Madison, WI, USA, 1997.
[32] K. Karrouchi, S. Fettach, Mukesh M. Jotani, A. Sagaama, S. Radi, H.A. Ghabbour, Y.N. Mabkhot, B. Himmi, M.E.A. Faouzi, N. Issaoui, Synthesis, crystal structure, hirshfeld surface analysis, DFT calculations, anti-diabetic activity and molecular docking studies of (E)-N'-(5-bromo-2-hydroxybenzylidene) isonicotinohydrazide, J. Mol. Struct. 1221 (2020) 128800.
[33] Frisch, M.J.; Trucks, G.W.; Schlegel, H.B.; Scuseria, G.E.; Robb, M.A.; Cheeseman, J.R.; Scalmani, G.; Barone, V.; Petersson, G.A.; Nakatsuji, H.; Li, X.; Caricato, M.; Marenich, A.V.; Bloino, J.; Janesko, B.G.; Gomperts, R.; Mennucci, B.; Hratchian, H.P.; Ortiz, J.V.; Izmaylov, A.F.; Sonnenberg, J.L.; Williams, F.; Ding, F.; Lipparini, F.; Egidi, J.; Goings, B.; Peng, A.; Petrone, T.; Henderson, D.; Ranasinghe, V.G.; Zakrzewski, J.; Gao, N.; Rega, G.; Zheng, W.; Liang, M.; Hada, M.; Ehara, K.; Toyota, R.; Fukuda, J.; Hasegawa, M.; Ishida, T.; Nakajima, Y.; Honda, O.; Kitao, H.; Nakai, T.; Vreven, K.; Throssell, J.A.; Montgomery Jr., J.E.; Peralta, F.; Ogliaro, M.J.; Bearpark, J.J.; Heyd, E.N.; Brothers, K.N.; Kudin, V.N.; Staroverov, T.A.; Keith, R.; Kobayashi, J.; Normand, K.; Raghavachari, A.P.; Rendell, J.C.; Burant, S.S.; Iyengar, J.; Tomasi, M.; Cossi, J.M.; Millam, M.; Klene, C.; Adamo, R.; Cammi, J.W.; Ochterski, R.L.; Martin, K.; Morokuma, O.; Farkas, J.B.; Foresman, D.J.; Fox, Gaussian 16 Rev. C.01, in, Wallingford, CT, 2016.
[34] M. Andersson, P. Uvdal, New scale factors for harmonic vibrational frequencies using the B3LYP density functional method with the triple-ζ basis set 6-311+G (d,p), J. Phys. Chem. A 109 (2005) 2937–2941.
[35] R. Ditchfield, Molecular orbital theory of magnetic shielding and magnetic susceptibility, J. Chem. Phys. 56 (1972) 5688–5691.
[36] K. Wolinski, J.F. Hinton, P. Pulay, Efficient implementation of the gauge-independent atomic orbital method for NMR chemical shift calculations, J. Am. Chem. Soc. 112 (1990) 8251–8260.

[37] J. Tomasi, B. Mennucci, R. Cammi, Quantum mechanical continuum solvation models, Chem. Rev. 105 (2005) 2999–3094.
[38] S. Wolff, D. Grimwood, J. McKinnon, M. Turner, D. Jayatilaka, M. Spackman, CrystalExplorer 3.0, University of Western Australia, Perth, 2012.
[39] G.M. Morris, R. Huey, W. Lindstrom, M.F. Sanner, R.K. Belew, D.S. Goodsell, A.J. Olson, AutoDock4 and AutoDockTools4: automated docking with selective receptor flexibility, J. Comput. Chem. 30 (2009) 2785–2791.
[40] T. Tagami, K. Yamashita, M. Okuyama, H. Mori, M. Yao, A. Kimura, Molecular basis for the recognition of long-chain substrates by plant alpha-glucosidases, J. Bio. Chem. 288 (2013) 19296–19303.
[41] V. Nahoum, R. Geneviève, V. Anton, P. Rougé, A. Puigserver, H. Bischoff, B. Henrissat, F. Payan, Crystal structures of human pancreatic α-amylase in complex with carbohydrate and proteinaceous inhibitors, Biochem. J. 346 (2000) 201–208.
[42] H.A. Abuelizz, E.H. Anouar, R. Ahmad, N.I.I.N. Azman, M. Marzouk, R. Al-Salahi, Triazoloquinazolines as a new class of potent α-glucosidase inhibitors: *in vitro* evaluation and docking study, PLoS ONE 14 (2019) e0220379.
[43] Y. El Bakri, E.H. Anouar, I. Marmouzi, K. Sayah, Y. Ramli, M. El Abbes Faouzi, E.M. Essassi, J.T. Mague, Potential antidiabetic activity and molecular docking studies of novel synthesized 3.6-dimethyl-5-oxo-pyrido[3,4-*f*][1,2,4]triazepino[2,3-*a*]benzimidazole and 10-amino-2-methyl-4-oxo pyrimido[1,2-*a*]benzimidazole derivatives, J. Mol. Model. 24 (2018) 179.
[44] K. Karrouchi, S.A. Brandán, Y. Sert, H. El-marzouqi, S. Radi, M. Ferbinteanu, M.E.A. Faouzi, Y. Garcia, M. Ansar, Synthesis, X-ray structure, Vibrational spectroscopy, DFT investigation and biological evaluation studies of (E)-N'-(4-(dimethylamino)benzylidene)-5-methyl-1H-pyrazole-3-carbohydrazide, J. Mol. Struct. 1219 (2020) 128541.
[45] K. Karrouchi, S.A. Brandán, Y. Sert, M. El Karbane, S. Radi, M. Ferbinteanu, Y. Garcia, M. Ansar, Synthesis, structural, molecular docking and spectroscopic studies of (E)-N'-(4-methoxybenzylidene)-5-methyl-1H-pyrazole-3-carbohydrazide, submitted to, J. Mol. Struct. 1225 (2020) 129072.
[46] K. Karrouchi, S.A. Brandán, M. Hassan, K. Bougrin, S. Radi, M. Ferbinteanu, Y. Garcia, M. Ansar, Synthesis, X-ray, spectroscopy, molecular docking and DFT calculations of (E)-N'-(2,4-dichlorobenzylidene)-5-phenyl-1H-pyrazole-3-carbohydrazide, J. Mol. Struct. 1228 (2020) 129714.